

# 1 **Characterization of the Particle Emission from Ships Operating at** 2 **Sea Using Unmanned Aerial Vehicles**

3 Tommaso F. Villa<sup>1</sup>, Reece Brown<sup>1</sup>, E. Rohan Jayaratne<sup>1</sup>, L. Felipe Gonzalez<sup>2</sup>, Lidia Morawska<sup>1</sup>, Zoran  
4 D. Ristovski<sup>1\*</sup>

5 <sup>1</sup> International Laboratory for Air Quality and Health (ILAQH), Queensland University of Technology (QUT), 2 George St,  
6 Brisbane QLD 4000

7 <sup>2</sup> Australian Research Centre for Aerospace Automation (ARCAA), Queensland University of Technology (QUT), 2 George  
8 St, Brisbane QLD 4000

9 *Correspondence to:* Zoran D. Ristovski (z.ristovski@qut.edu.au)

10 **Abstract.** This research demonstrates the use of an unmanned aerial vehicle (UAV) to characterize the gaseous (CO<sub>2</sub>) and  
11 particle (10 - 500 nm) emissions of a ship at sea. The field study was part of the research voyage “The Great Barrier Reef as a  
12 significant source of climatically relevant aerosol particles” on-board the RV Investigator around the Australian Great Barrier  
13 Reef. Measurements of the RV Investigator exhaust plume were carried out while the ship was operating at sea, at a steady  
14 engine load of 30%.

15 The UAV system was flown autonomously using several different programmed paths. These incorporated different altitudes  
16 and distances behind the ship in order to investigate the optimal position to capture the ship plume. Five flights were performed,  
17 providing a total of 27 horizontal transects perpendicular to the ship exhaust plume. Results show that the most appropriate  
18 altitude and distance to effectively capture the plume was 25 m above sea level and 20 m downwind.

19 Particle number emission factors (EF<sub>PN</sub>) were calculated in terms of number of particles emitted (#) per weight of fuel  
20 consumed (Kg fuel). Fuel consumption was calculated using the simultaneous measurements of plume CO<sub>2</sub> concentration.

21 The calculated EF<sub>PN</sub> was  $7.6 \pm 1.4 \times 10^{15} \text{ \#} \cdot \text{Kg}_{\text{fuel}}^{-1}$ , which is in line with those reported in the literature for ship emissions  
22 ranging from  $0.2 \times 10^{16} \text{ \#} \cdot \text{Kg}_{\text{fuel}}^{-1}$  to  $6.2 \times 10^{16} \text{ \#} \cdot \text{Kg}_{\text{fuel}}^{-1}$ .

23 This UAV system successfully assessed ship emissions to derive EF<sub>PN</sub> under real world conditions. This is significant as it  
24 provides a novel, inexpensive and accessible way to assess ship EF<sub>PN</sub> at sea.

## 25 **1. Introduction**

26 Shipping is the most significant contributor to international freight, with almost 80% of the worldwide merchandise trade by  
27 volume transported by ships in 2015 (UNCTAD, 2015). Emissions from this transportation mode are a significant contributor  
28 to air pollution, both locally and globally. Ships are a major pollutant source in areas surrounding harbours (Viana et al., 2014),  
29 with over 70% of emissions reaching 400 km inland (Fuglestad et al., 2009). In 2012 exhaust from diesel engines, the  
30 predominant source of ship power, was classified as a group 1 carcinogen by the International Agency for Research on Cancer  
31 (IARC). In 2007, pollution from ship exhaust was found to be responsible for approximately 60,000 cardiopulmonary and lung  
32 cancer deaths worldwide annually (Corbett et al., 2007a). Such emissions are also a strong climate forcing agent, contributing  
33 to global warming through the absorbance of solar and terrestrial radiation (Winnes et al., 2016; Hallquist et al., 2013a; Lack et  
34 al., 2011).

35 Despite these findings, emissions from shipping have consistently been subject to less regulation than those of land-based  
36 transport with ship emissions in international waters remaining one of the least regulated parts of the global transportation  
37 system (Cooper, 2001, 2005; Corbett and Koehler, 2003; Corbett and Farrell, 2002; Eyring et al., 2005; Streets et al.,  
38 1997; USEPA-OTAC, 2012). Currently, no specific restrictions for ship-emitted particulate matter (PM) exist, with the only  
39 regulated pollutants being NO<sub>x</sub> and SO<sub>2</sub>. The International Maritime Organization (IMO) recently revised the regulation of

40 these gaseous pollutants through the Annex VI of the International Convention for the Prevention of Pollution from Ships –  
41 the Marine Pollution Convention (MARPOL). The IMO expected that these regulations would lead to an indirect decrease in  
42 particle number (PN) concentration due to the reduction of NO<sub>x</sub> emissions and the use of fuel with lower sulphur content [14].  
43 However, it has been found that the use of some low sulphur fuels lead to increased PN concentrations at lower engine loads  
44 (Anderson et al., 2015), which stresses the importance for regulation specifically addressing particulate matter (PM).  
45 The majority of emitted PM is in the ultrafine size range, < 0.1 μm, which have been demonstrated to have a particularly  
46 significant impact on health and the environment (WHO, 2013). However, due to the lack in regulation, ultrafine particles, in  
47 terms of PN concentration, emitted from ships have remained unassessed in real world conditions. Quantifying PN  
48 concentration is critical to improve our understanding of shipping’s impact on health and climate (Chen et al., 2005; Cooper,  
49 2001; Corbett and Farrell, 2002; Isakson et al., 2001; Williams et al., 2009; Reda et al., 2015; Mueller et al., 2015; Anderson et  
50 al., 2015; Blasco et al., 2014; Ristovski et al., 2012; Corbett et al., 2007b). To achieve this, wide-scale evaluation of ship  
51 emission factors (EFs) is necessary. EFs are commonly expressed as the amount of pollutant (x) emitted per unit mass of fuel  
52 consumed g(x). (Kg fuel)<sup>-1</sup>. Different methods have been used to investigate ship EFs, including laboratory test-bench studies,  
53 on-board measurements, and measurement of ship emission plumes.  
54 Test-bench studies (Reda et al., 2015; Mueller et al., 2015; Anderson et al., 2015; Petzold et al., 2010; Petzold et al., 2008; Kasper  
55 et al., 2007) have been used to characterize emissions from different engines at various loads in laboratory conditions.  
56 However, engine performance and emissions have been shown to be different in real world operations when compared to  
57 laboratory studies. This calls for measurements of ship emissions in-situ to collect reliable data for EF calculations (Blasco et  
58 al., 2014; Murphy et al., 2009; Agrawal et al., 2008). To date, only a few studies have been undertaken on-board ships to  
59 calculate real emission factors (Juwono et al., 2013; Hallquist et al., 2013b). This is attributed to the prohibitive costs and time  
60 commitments of setting up and maintaining on-board measurement equipment on commercial ships. Airborne ship plume  
61 measurements (Westerlund et al., 2015; Schreier et al., 2015; Pirjola et al., 2014; Cappa et al., 2014; Beecken et al., 2014; Balzani  
62 Lööv et al., 2014; Berg et al., 2012; Lack et al., 2009; Lack et al., 2008; Sinha et al., 2003) offer an alternative method of in-situ  
63 measurements without requiring on-board monitoring stations. In the past the deployment cost of these systems, and the risks  
64 associated with manned aircrafts have limited their feasibility. However, this has recently changed with the rapid advances  
65 being made in commercially available Unmanned Aerial Vehicle (UAV) technology.  
66 Hexacopter UAVs have seen a wide scale increase in industry and research applications due to their ease of use and  
67 comparatively low cost (Malaver Rojas et al., 2015; Gonzalez et al., 2011; Brady et al., 2016). Used in conjunction with air  
68 monitoring equipment, these systems provide, for the first time, the ability to perform relatively simplistic and cost-effective  
69 airborne measurements of ship emissions. However, to date no studies have reported the use of a UAV system capable of  
70 collecting data to calculate the EF of PN concentration for ships at sea.  
71 This research utilized a customized hexacopter UAV carrying instruments for PN concentration and CO<sub>2</sub> measurements to  
72 derive  $EF_{PN}$ . The UAV system was deployed from the RV Investigator research vessel while at sea. Autonomous measurements  
73 of the RV investigators exhaust plume were taken over several flights at various altitudes and distances from the ship. Data  
74 collected was used to optimize the sampling flight path and successfully quantify the RV investigators EF for PN concentration.

## 75 **2. Methodology and Measurement system**

76 Measurements were conducted as part of the research voyage “The Great Barrier Reef as a significant source of climatically  
77 relevant aerosol particles” aboard the RV Investigator research vessel over a two day period of the 13 and 14 October 2016  
78 (day 1 and day 2). Measurements of PN and CO<sub>2</sub> concentration emitted by the RV Investigator were taken using a PN and CO<sub>2</sub>  
79 monitor mounted on a customized DJI EVO S800 hexacopter UAV (DJI, 2014).

## 80 2.1. The RV Investigator and the voyage

81 The RV Investigator is an ocean research vessel configured to enable a wide range of atmospheric, biological, geoscience and  
82 oceanographic research. The vessel is 94 m long, has a gross weight of 6,082 tons, a fuel capacity of 700 tons of ultra-low  
83 sulphur diesel fuel. It is powered by three 9 cylinder 3000 kW MaK diesel engines, each coupled to a 690V AC Generator.  
84 Ship propulsion is achieved using two 2600 kW L3 AC reversible propulsion motors powered by these generators. The RV  
85 Investigator can host up to 30 crew members and 35 researchers for a maximum voyage period of 60 days with a maximum  
86 cruising speed of 12 knots.

87 A suite of instrumentation for atmospheric research is available on the RV Investigator. This includes a radar system capable  
88 of collecting weather information within a 150 km radius of the vessel, and instruments measuring: sunlight parameters; aerosol  
89 composition, particle concentration and size distributions; cloud condensation nuclei; gas concentrations; and various other  
90 components of the atmosphere. These instruments are housed inside two dedicated on-board laboratories for aerosol and for  
91 atmospheric chemistry research. An atmospheric aerosol sample is continuously drawn into the laboratories for analysis  
92 through a specialized inlet fitted to the foremast of the ship. Of particular interest to this study, the ship contains a PICARRO  
93 (PICARRO Inc., Santa Clara, California, USA) G2401 analyser (Inc., 2017) that continuously measures CO<sub>2</sub>, CO, H<sub>2</sub>O and  
94 CH<sub>4</sub>. It has an operation range between 0-1000 ppm and a parts-per-billion sensitivity (ppb) for CO<sub>2</sub>.

95 The two day UAV measurement study was possible as part of the RV Investigator voyage “The Great Barrier Reef as a  
96 significant source of climatically relevant aerosol particles”, which started in Brisbane on the 28<sup>th</sup> of September 2016. The ship  
97 was used as both: a floating platform to allow launch and recovery of the UAV system; and as the source of an exhaust plume  
98 measured by the UAV system for EF calculation. During a several day stationary period on the Great Barrier Reef off the coast  
99 of Australia, it was possible to measure the ship plume under stable real world conditions over two consecutive days. One of  
100 the three ship engines was maintained at a steady engine load of 25 – 30 % of the maximum engine power during all  
101 measurements.

## 102 2.2. UAV system

103 Measurements of PN and CO<sub>2</sub> concentrations in the ship plume were performed using two commercial sensors mounted on-  
104 board a hexacopter UAV. The UAV used (Figure 1) is a composite material S800 EVO manufactured by DJI (DJI, 2014). The  
105 UAV is 800 mm wide and 320 mm in height, with an unloaded weight of 3.7 kg. Minimum and maximum take-off weights  
106 are 6.7 kg and 8 kg, respectively. The UAV contains a 16000 mAh LiPo 6 cell battery, which provides a hover time of  
107 approximately 20 min when operating at minimum take-off weight. The telemetry range of the UAV is 2 km, which was  
108 adequate to cover the desired sampling area (See Figure 2).

109 The payload consisted of a PN concentration and a CO<sub>2</sub> monitor mounted on-board underneath the UAV. Careful placement  
110 of the payload was required to prevent flight issues caused by an altered centre of gravity. Also included was a carbon fibre  
111 rod, which extended outward horizontally from the UAV. The sampling lines for the monitors were attached to the end of this  
112 rod to ensure that measurements were not affected by the downwash of the UAV rotors. The total weight of the payload was  
113 (1.2 kg), which allowed the UAV system to fly for 12-15 min before landing at the home point (A) (See Figure 2).

114 The S800 was used in conjunction with the DJI Wookong autopilot. The software provides an intuitive and easy to use interface  
115 where autonomous flight paths can be planned, saved, and uploaded into the UAV. In addition to this, the ground station allows  
116 for continuous, real-time monitoring of the status of the UAV during operation; which includes its longitude, latitude, altitude,  
117 waypoint tolerance and airspeed.

118 The DJI S800 was chosen for this study because it is designed to operate under the 20 kg all up weight (AUW) class of UAV.  
119 This reduces operational costs and avoid subjection to the tighter regulations of larger platforms. Small UAV cannot be  
120 operated above any person, or closer than 30 m of populated areas, houses and people. Furthermore, current Civil Aviation  
121 Safety Australia (CASA) regulations restrict the use of small UAV (2 and 20 kg) to visual line-of-sight daylight operation,

122 with a maximum altitude of approximately 120 m and within a radius of 3 nmi of an airport. UAVs in this category are not  
123 permitted for research unless the research institution has been granted a permit exception. These exceptions can be granted if  
124 the institution in question has or collaborates with an UAV operation team who must have: an experienced UAV pilot who is  
125 also radio controller specialist; a license for commercial UAV operation; and appropriate liability insurance (NPRM 1309OS  
126 - Remotely Piloted Aircraft Systems). Queensland University of Technology (QUT) has an unmanned operator certificate and  
127 four pilots who have UAV controller licenses.

## 128 2.2.1. Instrumentation

### 129 2.2.1.1. Instrumentation for PN concentration

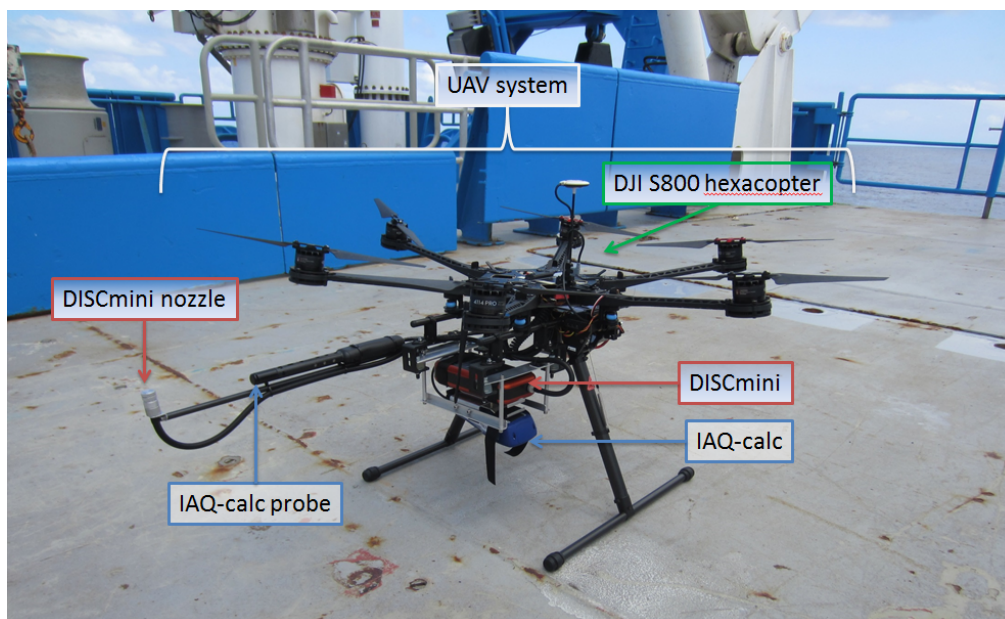
130 This study measured PN concentration using a Mini Diffusion Size Classifier (DISCmini), developed by the University of  
131 Applied Sciences, Windisch, Switzerland (Fierz et al., 2008). The DISCmini is a portable monitor used to measure  
132 concentration of particles in the 10-500 nm diameter size range, with a time resolution of up to 1s (1 Hz). It can measure PN  
133 concentrations between  $10^3$  and  $10^6$  N/cm<sup>3</sup>. Measurement accuracy is dependent upon the particle shape, size distribution, and  
134 number concentration. The advantages of using the DISCmini are its relatively small dimensions (180 x 90 x 40 mm), low  
135 weight (640 g, 780 g with the sampling probe, Figure 1) and long battery life of up to 8 hrs. These characteristics allow it to  
136 be easily integrated on the UAV.

### 137 2.2.1.2. Instrumentation for CO<sub>2</sub> concentration measurements

138 A TSI (TSI, Shoreview, Minnesota, United States) IAQ-calc 7545 model was chosen to measure CO<sub>2</sub> concentrations. Its sensor  
139 is based on a dual-wavelength NDIR (non-dispersive infrared) with a sensitivity range between 0 to 5,000 ppm and an accuracy  
140 of  $\pm 3.0\%$  of reading or  $\pm 50$  ppm (whichever is greater). The measurement resolution is 1 ppm with a maximum time resolution  
141 of 1s. Similar to the DISCmini, the advantages of using the IAQ-calc are: its small dimensions (178 x 84 x 44 mm); low weight  
142 (270 g, with batteries, significantly lower than the DISCmini), and a battery life of 10 hours.

143 The readings of the IAQ-calc for CO<sub>2</sub> were compared with those measured by the on-board PICARRO G2401 analyser.

144 Both the DISCmini and the IAQ-calc were tested and calibrated in the on-board laboratory using ambient aerosol  
145 measurements at sea prior to the commencement of the measurements (Figure S2 in the Supplementary Material). All data  
146 were logged with a 1 s time interval.



147  
148 **Figure 1. The UAV system with the on-board instrumentation: the DISCmini and the IAQ-calc.**

149

150 **2.3. Meteorological data**

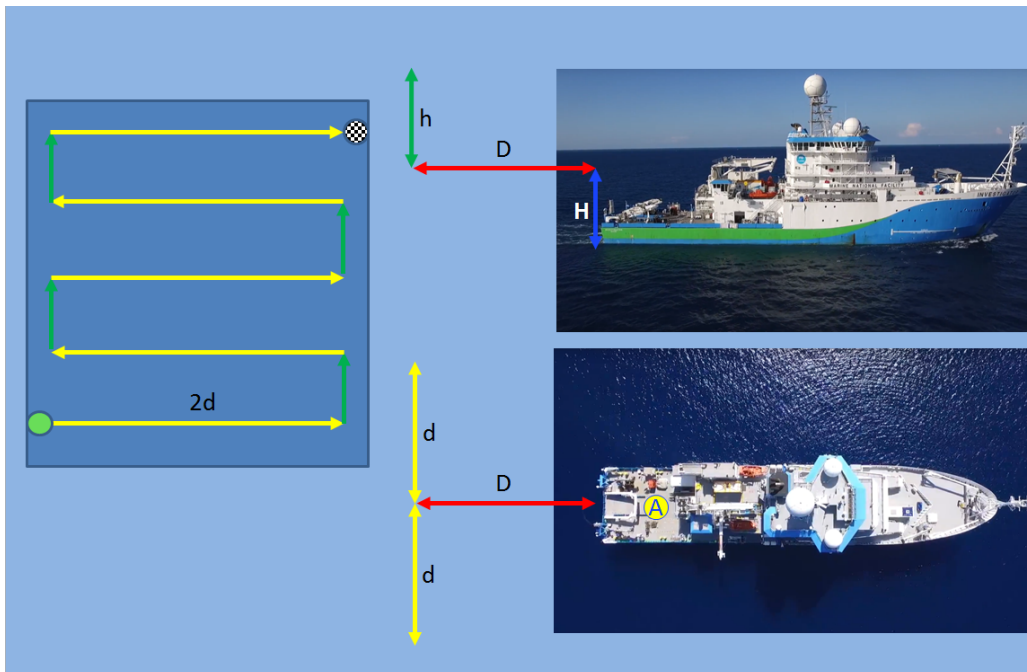
151 Meteorological data (including air temperature, relative humidity, atmospheric pressure, wind speed and direction) were  
152 recorded by the RV Investigators on-board instrumentation during the entire voyage with a 60 s time interval, 24/h a day.

153 **2.4. Study design**

154 During the two measurement days of this study, the vessel was heading into the wind whilst idling the UAV missions at sea.  
155 This positioning caused the exhaust plume to extend downwind, directly behind the ship. The UAV system was launched off  
156 the back deck, autonomously sampling at varying altitudes and distances into the downwind plume. Flight speed of the UAV  
157 was 1.5 m/s, the minimum for the S800.

158 Day 1 was used to optimise the study design, focusing on finding the flight path most suitable to capture the ship plume. Figure  
159 2 shows the programmed flight path, which consisted of a continuous flight beginning at a distance ( $D$ ) and from an altitude  
160 ( $H$ ) above the surface. Point A, located on the back deck of the RV Investigator, represents the ‘home point’. In UAV  
161 terminology this refers to the position where the UAV system takes off and lands. The UAV system was programmed to move  
162 horizontally by a distance ( $2d$ ), perpendicular to the ship, then climb vertically for 10 m ( $h$ ) before flying in the opposite  
163 horizontal direction for the same distance ( $2d$ ). The UAV was then programmed to climb another 10 m ( $h$ ) before repeating  
164 this pattern until the UAV reached an altitude of 65 m above the ocean. During day 1, the UAV system followed three different  
165 flight paths, each one with both a different distance  $D$  behind the ship (20, 50 and 100 m), and a different horizontal distance  
166  $2d$  (50, 100 and 150 m).

167 The optimised flight path for day 2 started 20 m behind the ship and 25 m above the surface, with no altitude variation. The  
168 UAV path was limited to a continuous horizontal flight of 50 m ( $2d$ ) at steady speed of  $2 \text{ m s}^{-1}$ . This path and flying speed  
169 allowed up to 4 horizontal transects to capture the ship plume.



170

171 **Figure 2. Flight path used to capture the plume:  $H$  - height from the ocean,  $D$  – distance behind the ship to the flight beginning point,**  
172  **$h$  – rising altitude after the horizontal transect,  $2d$  – full length of the horizontal transect**

173 **2.5. Experimental procedure**

174 The UAV can fly either manually or autonomously. As a safety precaution, every take-off and landing was performed using  
175 the manual flight mode. Once in the air, the UAV was switched to autonomous flight mode, allowing the platform to follow  
176 the pre-programmed flight path discussed in the previous section. The flight path consisted of waypoints, which are three-



177 dimensional GPS points that dictate the position of the UAV along the flight path. The waypoints and flight plans for each  
178 flight were programmed using the aforementioned DJI Wookong ground station software. The DISCmini and the IAQ-calc  
179 were fitted on the underside of the UAV at the beginning of each measuring day. Five flights were performed across the two  
180 measurement days, providing a total of 27 horizontal transects perpendicular to the ship's exhaust plume.

## 181 2.6. Emission factors

182 The calculation of an emission factor for particle number concentration ( $EF_{PN}$ ) from the collected ship plume measurements  
183 was performed using Eq. (1). This method has previously been used for ship (Westerlund et al., 2015), road vehicle (Hak et  
184 al., 2009) and aircraft (Mazaheri et al., 2009) emissions. The measured values of PN concentration were related to the amount  
185 of fuel consumed by the engine in question through the use of the simultaneous measurements of CO<sub>2</sub> concentration taken by  
186 the UAV. This was achieved by using a published value for a ship emission factor of CO<sub>2</sub> ( $EF_{gas}$ ) of 3.2 Kg CO<sub>2</sub> (Kg fuel)<sup>-1</sup>  
187 (Hallquist et al., 2013b; Hobbs et al., 2000).

188 Eq.(1).

$$189 \quad EF_{PN} = \frac{\Delta PN}{\Delta gas} \times EF_{gas} \quad (1)$$

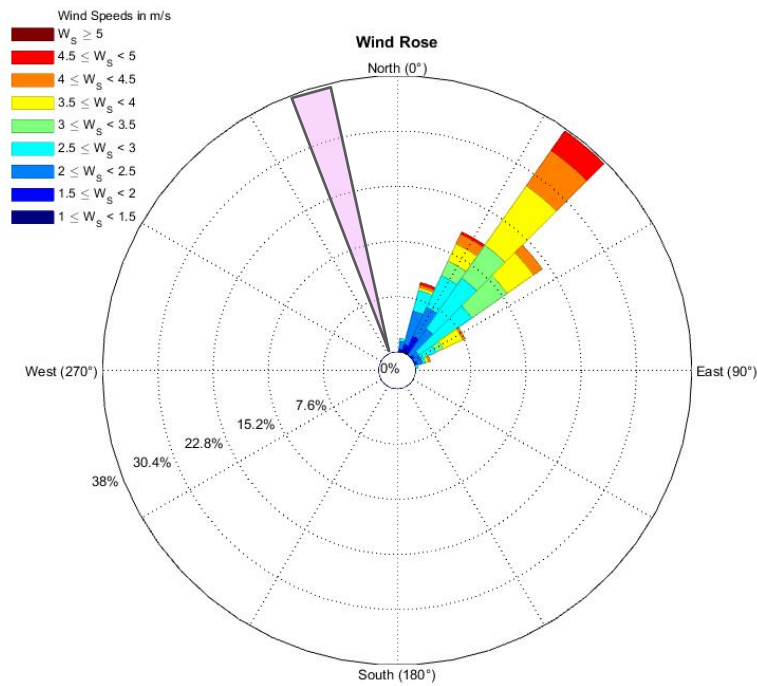
190 The  $\Delta PN$  and  $\Delta gas$  in Eq. (1) represent the maximum particle concentration change above background in the measured  
191 particle number and CO<sub>2</sub> concentrations, respectively. The DISCmini measurements were corrected against a reference CPC.  
192 For each transect data series of PNC and CO<sub>2</sub>, the averaged background concentration were subtracted from the peak data  
193 corresponding to measurements inside the plume. The corrected peak data series were then fit with a Gaussian curve using the  
194 inbuilt Matlab curve fitting application. The least absolute residuals (LAR) condition was used as this most closely fits the  
195 curve to the highest magnitude data points in the series. The maximum peak height of the fitted Gaussian curves were used as  
196  $\Delta PNC$  and  $\Delta CO_2$  in the calculation of emission factors for each transect.

## 197 3. Results and Discussion

### 198 3.1. Meteorological and Investigator data

199 Wind conditions were very stable during both day 1 and day 2, following one main pattern for the entire flight time. The wind  
200 speed ranged from 3 - 13 m s<sup>-1</sup>. The wind direction was predominantly from the NE during day 1 and ESE during day 2. The  
201 wind rose graphs in Figure 3a and 3b illustrate the wind data recorded with the on-board weather instrumentation during all  
202 horizontal transects flown during day 1 and 2 respectively. The prevalent wind direction was ESE, which corresponded to the  
203 heading of the RV Investigator (indicated by the rose triangle). The wind direction changed occasionally to E during the flight,  
204 causing the UAV to fail to capture the RV Investigator plume during some transects. As a result, 2 of the 8 horizontal transects  
205 collected on day 2 were excluded from the analysis.

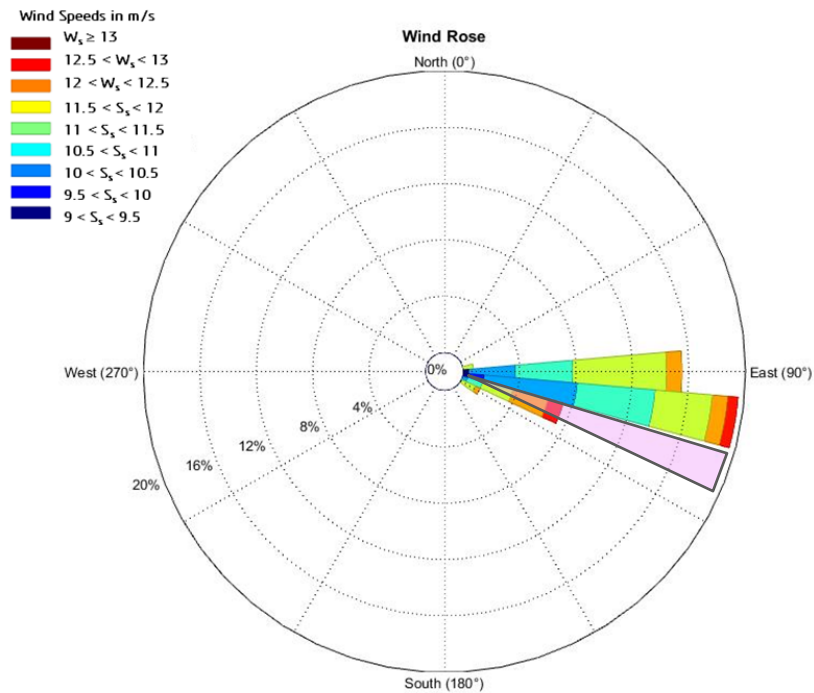
206



207

208 Figure 3a – Wind rose showing wind speed and direction during day 1. Rose triangle shows RV Investigator direction during the  
 209 measurements.

210



211

212 Figure 3b – Wind rose showing wind speed and direction during day 2 optimized flight. Rose triangle shows RV Investigator  
 213 direction during the measurements.

214 **3.2. UAV system horizontal transects inside and outside the plume**

215 The UAV system acquired data for a total of 27 horizontal transects for day 1 and day 2. Data were collected at altitudes  
 216 between 25 m and 65 m above the water surface. During day 1 the plume was captured once when the UAV was at 25 m

217 altitude and 20 m downwind of the ship; and again at both 25 and 35 m altitude 100 m downwind of the ship. These  
 218 observations lead to the optimized flight used on day 2, which started downwind at 25 m above the surface and 20 m behind  
 219 the ship. On day 2 the UAV system successfully captured the plume during 6 of the 8 transects performed. Across the two  
 220 days this lead to a total of 9 transects that captured the plume and which have been considered for discussion, shown in Table  
 221 1.

222

Measuring day	Altitude	Distance behind the Investigator	Number of transects
Day 1	25 m	20 m	1
*Day 1	25 m	100 m	1
Day 1	35 m	100 m	1
Day 2	25 m	20 m	6

223

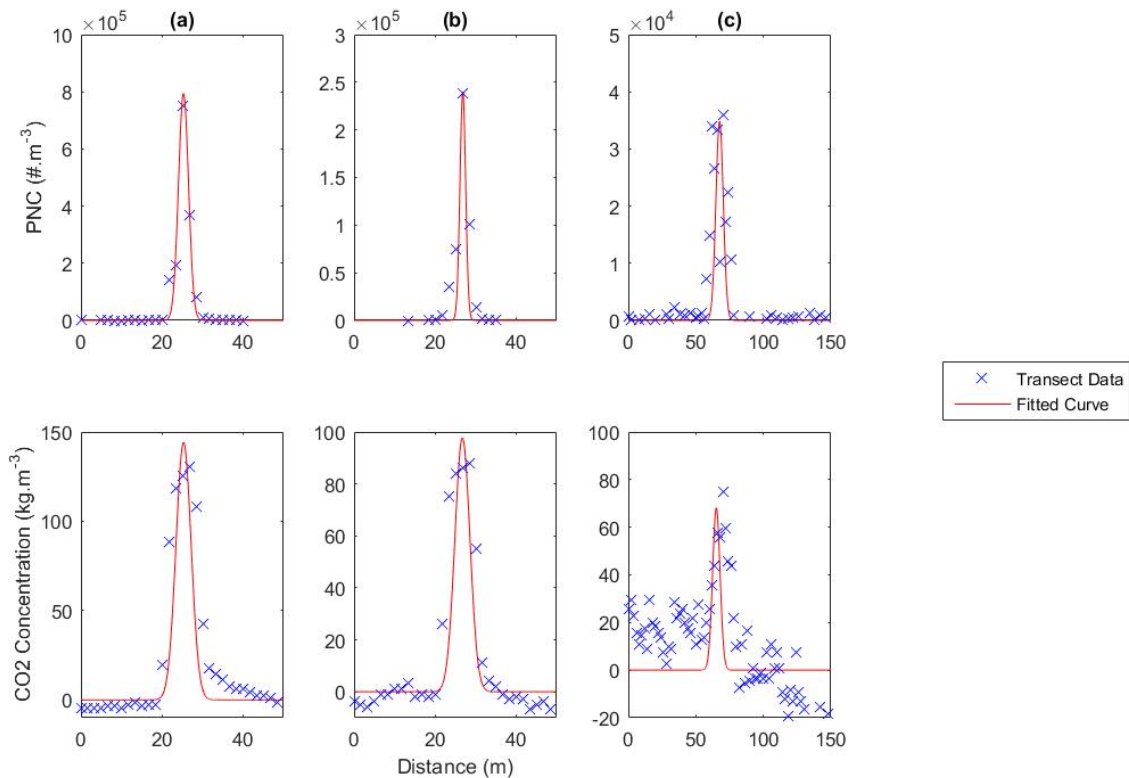
224 **Table 1** – Specifications of the transects considered for the data analysis. The (\*) indicates the transect of Day 1 of which PN  
 225 concentration and CO<sub>2</sub> profiles are presented in Figure 4.

226

227 Figure 4 shows the PN concentration and CO<sub>2</sub> profiles, collected during two (a; b) transects on day 2, and (c) during one  
 228 transect of day 1 (Spec. in Table 1, Day1\*).

229 The PN concentration profiles for the (a) and (b) transects in Figure 4 show that the concentration varied by five orders of  
 230 magnitude between the outside and inside the plume, while the CO<sub>2</sub> profiles show an increase up to 140 ppm above the  
 231 background.

232 The profiles in (c) show that the PN concentration was four orders of magnitude greater inside the plume at 100 m behind the  
 233 ship and that the CO<sub>2</sub> concentration was up to 70 ppm higher inside the plume.



234



235 Figure 4 – (a) and (b) show the measured PN and CO<sub>2</sub> concentration profiles and fitted Gaussian curves for two different transects  
 236 20 m behind the ship 25 m above the surface during day 2. (c) shows the PN and CO<sub>2</sub> concentration profiles and fitted Gaussian  
 237 curves collected during flight 3 of day 1 at 100 m behind the ship, 25 m above the surface.

238

239 Figure 4 (a) and (b) both show transects at 25 m altitude and 20 m behind the ship. Both the PN concentration and CO<sub>2</sub>  
 240 measurements show clear, single peaks as the UAV crosses the plume. As a consequence, these transects show a good fit with  
 241 the corresponding Gaussian distribution curves with R<sup>2</sup> values of above 0.9 for both PNC and CO<sub>2</sub>. In contrast Figure 4 (c)  
 242 shows substantially less defined, wider peaks with lower pollutant concentrations. This is attributed to a difference in flight  
 243 paths, with Figure 4 (c) representing data from a transect 100 m behind the ship. The additional time between emission and  
 244 sampling has allowed the plume to broaden, become less homogenous, and take on a skewed cross-section. This results in a  
 245 significantly lower R<sup>2</sup> value for the fitted Gaussian curves, with a value of 0.4998 for the CO<sub>2</sub> data in this transect. Therefore,  
 246 whilst the 100 m transect does provide more data points inside the plume, the randomized variations inside the plume lead to  
 247 less accurate calculations of emission factors.

248 Of further note in Figure 4, the maximum PN concentrations measured in (a) ( $7.5 \times 10^5 \# \cdot \text{cm}^{-3}$ ) is approximately three times  
 249 greater than those in (b) ( $2.4 \times 10^5 \# \cdot \text{cm}^{-3}$ ) and the CO<sub>2</sub> concentrations in (a) are 43 ppm greater than (b). The transect flight plan  
 250 and ship engine load remained constant throughout these measurements. The variations between (a) and (b) are attributed to  
 251 several factors which reduce the effectiveness of the UAV transect for capturing the plume. Slight changes in ambient  
 252 conditions such as temperature, wind direction and intensity will alter the path of the plume as it moves away from the ship.  
 253 The UAVs automated flight path cannot account for these variations. Therefore, the degree to which the UAV enters the plume,  
 254 and thus the concentrations it measures, will be different on each transect. Both CO<sub>2</sub> and PN concentration measurements will  
 255 be similarly affected by this variance. However, differences in instrument response rates in conjunction with these variances  
 256 will be one of the major contributors to variations in calculated emission factors.

### 257 3.3. PN Emission Factors

258 Table 2 shows the distance and altitude of each transect, the R<sup>2</sup> values of the fitted Gaussian curves for PNC and CO<sub>2</sub> data, the  
 259 calculated values of  $\Delta\text{PNC}$  and  $\Delta\text{CO}_2$ , and the calculated EF<sub>PN</sub>.

Day	Dist/Alt (m)	R <sup>2</sup> <sub>PNC</sub>	R <sup>2</sup> <sub>CO<sub>2</sub></sub>	$\Delta\text{PNC}$ (#.m <sup>-3</sup> )	$\Delta\text{CO}_2$ (kg.m <sup>-3</sup> )	EF <sub>PN</sub> (#.kg <sub>fuel</sub> <sup>-1</sup> )
1	100/25	0.9586	0.4998	5.05E+11	9.35E-05	1.73E+16
	100/35	0.4767	0.8967	4.8E+10	1.34E-04	1.15E+15
	20/25	0.9856	0.8915	1.09E+11	7.74E-05	4.52E+15
2	20/25	0.9842	0.9518	1.06E+12	2.83E-04	1.20E+16
	20/25	0.9852	0.8838	3.3E+11	1.92E-04	5.51E+15
	20/25	0.9489	0.9246	1.78E+11	1.11E-04	5.16E+15
	20/25	0.9721	0.8965	3.6E+11	2.23E-04	5.18E+15
	20/25	0.9508	0.8473	1.47E+11	1.31E-04	3.59E+15
	20/25	0.8517	0.6743	1.01E+11	9.68E-05	3.32E+15

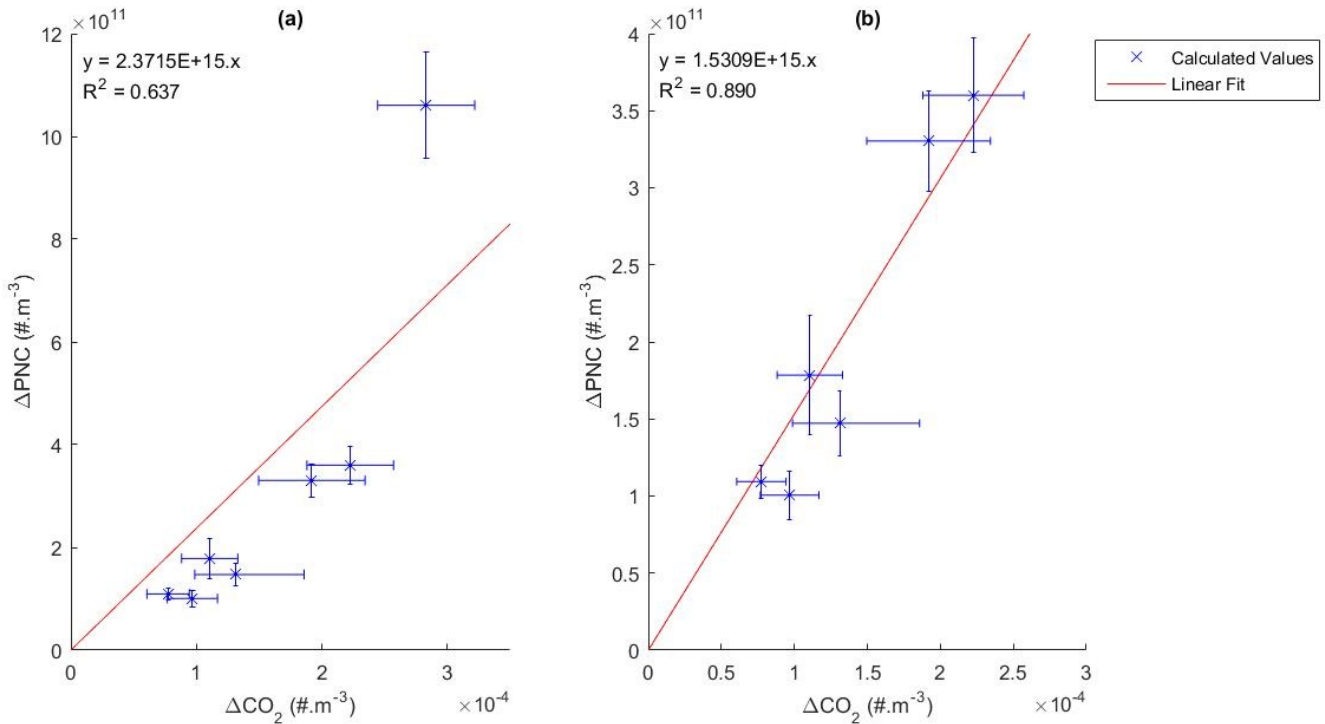
260

261 Table 2 – Transect flight days and details, R<sup>2</sup> values for the Gaussian curve fits to both PNC and CO<sub>2</sub> data,  $\Delta\text{PNC}$  and  $\Delta\text{CO}_2$   
 262 concentration emission/rate of the RV Investigator, and calculated Emission Factors for PN.

263

264 The calculated EF<sub>PN</sub> values for the RV Investigator ranged from  $1.15 \times 10^{15}$  to  $1.73 \times 10^{16} \# \cdot \text{kg}_{\text{fuel}}^{-1}$ . The two 100 m transects  
 265 provided the worst Gaussian fits as well as the highest and lowest calculated emission factors. This indicates that it is important  
 266 to filter out transects with data which does not fit the expected Gaussian distribution suitably as they can generate significant

267 error. To this end, the 100 m transects were excluded from further analysis.  $\Delta$ PNC and  $\Delta$ CO<sub>2</sub> values for remaining transects  
 268 were plotted against each other as shown in Figure 5.



269

270 **Figure 5 –(a)  $\Delta$ PNC against  $\Delta$ CO<sub>2</sub> with 95% confidence interval for the six transects considered for the data analysis. (b)  $\Delta$ PNC**  
 271 **against  $\Delta$ CO<sub>2</sub> with 95% confidence interval with the removal of the outlier transect from the first flight of day 2**

272

273 Figure 5 (a) and (b) show the plots of the remaining transects  $\Delta$ PNC against  $\Delta$ CO<sub>2</sub> with and without the values of the first  
 274 flight of day 2. This transect represents a clear outlier in the linear trend, with the  $R^2$  value of the linear fit increasing from  
 275 0.637 to 0.890 with its exclusion. Furthermore, whilst the linear fit falls within the confidence interval of only one point in (a),  
 276 it falls within all data points confidence intervals in (b). This occurs despite both  $R^2$  values for the fitted Gaussians of this  
 277 transect being very high ( $R^2_{\text{PNC}} = 0.9842$ ,  $R^2_{\text{CO}_2} = 0.9518$ ). This highlights a limitation with this methodology which can be  
 278 best observed in the difference between Figure 4 (a) and (b). The combination of UAV velocity, sampling rate and response  
 279 time of the DISCmini results in the PNC transect data having only one data point defining the peak height of the transect.  
 280 Relying on a single sample point leads to the potential for random instrumentation effects heavily biasing results in a way  
 281 which does not strongly impact the  $R^2$  values of Gaussian fits used to identify successful transects. Therefore, it is unclear  
 282 whether this is a variation in the ship emissions or an instrumentation error.

283 The slope and standard error of the linear fit for Figure 4 (a) was input unto Equation 1 to calculate an overall emission factor  
 284 of  $7.6 \pm 1.4 \times 10^{15} \# \cdot \text{kg}_{\text{fuel}}^{-1}$ . As presented in Table 3, this value is comparable with those reported in the literature for cruise  
 285 and cargo ship plumes; which range from  $0.2 \times 10^{16}$  to  $6.2 \times 10^{16} \# \cdot \text{kg}_{\text{fuel}}^{-1}$  { #45;Alföldy, 2013 #52;Beecken, 2014  
 286 #34;Jonsson, 2011 #53;Juwono, 2013 #29;Lack, 2011 #7;Lack, 2009 #37;Pirjola, 2014 #32;Sinha, 2003 #39;Westerlund, 2015  
 287 #30}

288

Reference	Platform	EFPN (#.kg <sub>fuel</sub> <sup>-1</sup> )	Number of ships	Location
This Study	UAV	$7.6 \pm 1.4 \times 10^{15}$	1	Open Water
Westerlund et al. (2015)	Land Based	$2.35 \pm 0.20 \times 10^{16}$	154	Harbor, Ship Channel
Beecken et al. (2014)	Airborne	$1.8 \pm 1.3 \times 10^{16}$	174	Open Water
Pirjola et al. (2014)	Land Based	$0.32 \times 10^{16}$	11	Harbor, Ship Channel
Alföldy et al (2013)	Land Based	$0.8 \times 10^{16}$	497	Harbor
Juwono et al. (2012)	On Board	$0.22 \times 10^{16}$	2	Harbor, Ship Channel
Jonsson et al. (2011)	Land Based	$2.55 \pm 0.11 \times 10^{16}$	734	Harbor
Lack et al. (2009)	Ship	$0.71 \pm 0.55 \times 10^{16}$ (>13nm)* $1.27 \pm 0.95 \times 10^{16}$ (>5nm)**	172 165	Open Water, Shipping Channel
Lack et al. (2011)	Airborne	$1.0 \pm 0.2 \times 10^{16}$	1	Open Water
Sinha et al. (2003)	Airborne	$6.2 \pm 0.6 \times 10^{16}$	2	Open Water

289

290 **Table 3 – Comparison of the Emission Factor for the RV Investigator found in this study with other relevant values found in**  
 291 **literature. \* P<sub>NEF</sub> for particles above 13nm. \*\* P<sub>NEF</sub> for particles above 5nm.**

292 The calculated  $EF_{PN}$  for the Investigator was lower compared to those reported by Beecken et al. (Beecken et al., 2014) for  
 293 passenger ships while accelerating ( $0.91 \pm 0.18 \times 10^{16}$  #.Kg<sub>fuel</sub><sup>-1</sup>). However, the RV Investigator measurements were undertaken  
 294 whilst its engine was under 30% load. Accelerating ships will typically be under higher engine loads and hence have a  
 295 correspondingly higher  $EF_{PN}$  (Westerlund et al., 2015), which explains part of this discrepancy. Furthermore, the RV  
 296 Investigator has high efficiency engines and utilizes ultra-low sulphur diesel fuel. Studies have shown that similar diesel  
 297 engines burning fuel of this type have lower  $EF_{PN}$  than the same engine with higher sulphur content diesel (Chu-Van et al.,  
 298 2017). Similar quality fuels used in the ground transport industry have yielded similar values of  $EF_{PN}$ , ranging from  $4.8 \times 10^{14}$   
 299 ( $25\%$  engine load) to  $7.2 (100\% \text{ engine load}) \times 10^{15}$  #.Kg<sub>fuel</sub><sup>-1</sup> (Jayaratne et al., 2009).

### 300 3.4. Instrumentation Limitations

301 Lightweight UAVs present an opportunity to achieve aerial measurements at significantly less upfront and operational costs  
 302 than fixed wing and manned aerial vehicles. Lightweight UAVs can be deployed faster with limited or no required launch and  
 303 landing area compared to their manned and fixed wing counterparts. Yet, their primary disadvantage, particularly in this  
 304 application, is a severely limited payload weight. To overcome this limitation, this project used the lightweight and portable  
 305 DICSmini and IAQ-calc sensors. However, these instruments have lower sensitivities and greater uncertainties when compared  
 306 to a high accuracy CPC and CO<sub>2</sub> monitor for measurements, which can influence results.

307 The DISCmini has a manufacturer listed measurement cut-off size of 10 nm. A previous study listed in Table 3 (Lack, Corbett  
 308 et al. 2009) shows that the cut-off size of instruments used to measure PNC is directly linked to the value of  $EF_{PN}$ , with the  
 309 measured  $EF_{PN}$  doubling when the cut-off size is changed from 13 nm to 5 nm due to the large number of particles in this size  
 310 range. This may have been another contributing factor to the  $EF_{PN}$  measured in this study being in the lower end of measured  
 311 values in literature.

312 The two 100m transects were not accounted for in the final calculation of  $EF_{PN}$  due to their poor Gaussian curve fits. Whilst  
 313 this has been attributed to the skewing of the plume at this distance, the limitations of the instrumentation could also have  
 314 contributed. The lower concentrations of CO<sub>2</sub> at this distance result in the difference above background inside the plume being  
 315 the same order of magnitude as the manufacturer specified error margin. Hence, the variability in the plume either side of the  
 316 central peak as shown in figure 4 (c) could be due in part to instrumentation error.

317 Calibrations of sensors in this study were performed by comparison with reference instruments for ambient measurements at  
318 sea. Ideally, calibration should be performed with in-plume measurements, however it was not possible to access the plume  
319 with reference instrumentation on board the ship. Whilst this study provides a successful proof of concept with consistent  
320 results over multiple days and flights, a validation study is needed. This should include independent measurements of  $EF_{PN}$   
321 using other established methodologies to ascertain more precise correction factors and uncertainties.

## 322 4. Summary and conclusion

323 The UAV system used in this study successfully measured PN and CO<sub>2</sub> concentrations from the exhaust plume of the RV  
324 Investigator whilst operating at sea. Several different flight paths were tested and an optimal transect flying perpendicular to  
325 the plume at a distance of 20 meters from the ship was adopted. The  $EF_{PN}$  calculated for the RV investigator  $7.6 \pm 1.4 \times 10^{15}$   
326 #.kg<sub>fuel</sub><sup>-1</sup> at a constant 30% engine load. This  $EF_{PN}$  was in agreement with values reported in literature, indicating this novel  
327 UAV system has potential for  $EF_{PN}$  quantification pending further evaluation.

328 In comparison with other methods, the UAV system presented provides a cost effective and accessible solution for the rapid  
329 measurement and quantification of ship  $EF_{PNS}$ . Its ability for deployment both in harbour and at sea, coupled with the possibility  
330 of altering its flight path to account for variances in wind conditions; gives this UAV system a distinct advantage over ground  
331 based and manned aerial vehicles. Furthermore, the UAV can sample considerably closer to the plume emission source than  
332 other methodologies, providing higher concentration measurements for the calculation of  $EF_{PN}$ .

333 Whilst further validation is necessary, results present here indicate that this UAV system has the potential to be used a low  
334 cost tool for quantification of ultrafine particle emission factors from commercial shipping. This is critical to improve our  
335 understanding of shipping's impact on climate and health.

### 336 4.1. Recommendations

337 The potential of this UAV system extend far beyond what is described here. This study is intended as both: a proof of concept;  
338 and to provide useful information both for the future of this project, as well as any other UAV sampling systems being  
339 developed. The most significant improvement to the method described would be the use a UAV with a lower minimum  
340 airspeed. This would allow for more data points per transect and would minimize the impact potential outliers in  
341 instrumentation data. Other related improvements to this include: the use of different sensors with higher response rates; and  
342 additional flightpath investigations to find an optimal transect distance which provides the broadest plume cross-section,  
343 without the plume becoming distorted and impacting accuracy.

344 Further optimization of the transect approach is also possible. After location of the plume the system could be set to make  
345 several repeat passes across the plume in rapid succession to increase the sample size. Another alternative would involve the  
346 UAV hovering inside the plume over a period of time collecting a continuous series of measurements from the centre of the  
347 plume. These methods would both require real time sensor feedback to the UAV pilot and potentially adaptive autonomous  
348 controls to achieve a suitable result. This methodology could also be expanded to measure other important ship emission  
349 factors, including NO<sub>x</sub> and volatile organic compounds (VOCs).

## 350 Acknowledgements

351 The authors would like to acknowledge the ARCAA Operations Team (Dirk Lessner, Gavin Broadbent) who operated the  
352 Unmanned Aerial Vehicle (S800). This research was supported by the Australian Research Council Discovery Grant  
353 DP150101649 and the Marine National Facility. The authors would like to thank the Captain and the crew of the RV



354 Investigator as well as the on board MNF support staff as without their support and effort this research would not have been  
355 possible.

## 356 Reference

- 357 NPRM 1309OS - Remotely Piloted Aircraft Systems: [https://www.casa.gov.au/standard-page/nprm-1309os-remotely-piloted-aircraft-](https://www.casa.gov.au/standard-page/nprm-1309os-remotely-piloted-aircraft-systems?WCMS%3ASTANDARD%3A%3Apc=PC_102028)  
358 [systems?WCMS%3ASTANDARD%3A%3Apc=PC\\_102028](https://www.casa.gov.au/standard-page/nprm-1309os-remotely-piloted-aircraft-systems?WCMS%3ASTANDARD%3A%3Apc=PC_102028).
- 359 Agrawal, H., Malloy, Q. G. J., Welch, W. A., Wayne Miller, J., and Cocker Iii, D. R.: In-use gaseous and particulate matter emissions from  
360 a modern ocean going container vessel, *Atmospheric Environment*, 42, 5504-5510, <http://dx.doi.org/10.1016/j.atmosenv.2008.02.053>, 2008.
- 361 Anderson, M., Salo, K., Hallquist, Å. M., and Fridell, E.: Characterization of particles from a marine engine operating at low loads,  
362 *Atmospheric Environment*, 101, 65-71, <http://dx.doi.org/10.1016/j.atmosenv.2014.11.009>, 2015.
- 363 Balzani Lööf, J. M., Alfoldy, B., Gast, L. F. L., Hjorth, J., Lagler, F., Mellqvist, J., Beecken, J., Berg, N., Duyzer, J., Westrate, H., Swart,  
364 D. P. J., Berkhout, A. J. C., Jalkanen, J. P., Prata, A. J., Van Der Hoff, G. R., and Borowiak, A.: Field test of available methods to measure  
365 remotely SO<sub>x</sub> and NO<sub>x</sub> emissions from ships, *Atmospheric Measurement Techniques*, 7, 2597-2613, [http://dx.doi.org/10.5194/amt-7-2597-](http://dx.doi.org/10.5194/amt-7-2597-2014)  
366 [2014](http://dx.doi.org/10.5194/amt-7-2597-2014), 2014.
- 367 Beecken, J., Mellqvist, J., Salo, K., Ekholm, J., and Jalkanen, J. P.: Airborne emission measurements of SO<sub>2</sub>, NO<sub>x</sub> and particles from  
368 individual ships using a sniffer technique, *Atmospheric Measurement Techniques*, 7, 1957-1968, [http://dx.doi.org/10.5194/amt-7-1957-](http://dx.doi.org/10.5194/amt-7-1957-2014)  
369 [2014](http://dx.doi.org/10.5194/amt-7-1957-2014), 2014.
- 370 Berg, N., Mellqvist, J., Jalkanen, J. P., and Balzani, J.: Ship emissions of SO<sub>2</sub> and NO<sub>2</sub>: DOAS measurements from airborne platforms,  
371 *Atmospheric Measurement Techniques*, 5, 1085-1098, <http://dx.doi.org/10.5194/amt-5-1085-2012>, 2012.
- 372 Blasco, J., Duran-Grados, V., Hampel, M., and Moreno-Gutierrez, J.: Towards an integrated environmental risk assessment of emissions  
373 from ships' propulsion systems, *Environment international*, 66, 44-47, <http://dx.doi.org/10.1016/j.envint.2014.01.014>, 2014.
- 374 Brady, J. M., Stokes, M. D., Bonnardel, J., and Bertram, T. H.: Characterization of a Quadrotor Unmanned Aircraft System for Aerosol-  
375 Particle-Concentration Measurements, *Environmental Science & Technology*, 50, 1376-1383, 10.1021/acs.est.5b05320, 2016.
- 376 Cappa, C. D., Williams, E. J., Lack, D. A., Buffaloe, G. M., Coffman, D., Hayden, K. L., Herndon, S. C., Lerner, B. M., Li, S. M., Massoli,  
377 P., McLaren, R., Nuaaman, I., Onasch, T. B., and Quinn, P. K.: A case study into the measurement of ship emissions from plume intercepts  
378 of the NOAA ship Miller Freeman, *Atmos. Chem. Phys.*, 14, 1337-1352, <http://dx.doi.org/10.5194/acp-14-1337-2014>, 2014.
- 379 Chen, G., Huey, L. G., Trainer, M., Nicks, D., Corbett, J., Ryerson, T., Parrish, D., Neuman, J. A., Nowak, J., Tanner, D., Holloway, J.,  
380 Brock, C., Crawford, J., Olson, J. R., Sullivan, A., Weber, R., Schaufli, S., Donnelly, S., Atlas, E., Roberts, J., Flocke, F., Hübler, G., and  
381 Fehsenfeld, F.: An investigation of the chemistry of ship emission plumes during ITCT 2002, *Journal of Geophysical Research: Atmospheres*,  
382 110, D10S90, 10.1029/2004JD005236, 2005.
- 383 Chu-Van, T., Ristovski, Z., Pourkhesalian, A. M., Rainey, T., Garaniya, V., Abbassi, R., Jahangiri, S., Enshaei, H., Kam, U. S., Kimball, R.,  
384 Yang, L., Zare, A., Bartlett, H., and Brown, R. J.: On-board measurements of particle and gaseous emissions from a large cargo vessel at  
385 different operating conditions, *Environmental Pollution*, <https://doi.org/10.1016/j.envpol.2017.11.008>, 2017.
- 386 Cooper, D. A.: Exhaust emissions from high speed passenger ferries, *Atmospheric Environment*, 35, 4189-4200,  
387 [http://dx.doi.org/10.1016/S1352-2310\(01\)00192-3](http://dx.doi.org/10.1016/S1352-2310(01)00192-3), 2001.
- 388 Cooper, D. A.: HCB, PCB, PCDD and PCDF emissions from ships, *Atmospheric Environment*, 39, 4901-4912,  
389 <http://dx.doi.org/10.1016/j.atmosenv.2005.04.037>, 2005.
- 390 Corbett, J. J., and Farrell, A.: Mitigating air pollution impacts of passenger ferries, *Transportation Research Part D: Transport and*  
391 *Environment*, 7, 197-211, [http://dx.doi.org/10.1016/S1361-9209\(01\)00019-0](http://dx.doi.org/10.1016/S1361-9209(01)00019-0), 2002.
- 392 Corbett, J. J., and Koehler, H. W.: Updated emissions from ocean shipping, *Journal of Geophysical Research: Atmospheres*, 108, 4650,  
393 10.1029/2003JD003751, 2003.
- 394 Corbett, J. J., Winebrake, J. J., Green, E. H., Kasibhatla, P., Eyring, V., and Lauer, A.: Mortality from Ship Emissions: A Global Assessment,  
395 *Environmental Science & Technology*, 41, 8512-8518, 10.1021/es071686z, 2007a.
- 396 Corbett, J. J., Winebrake, J. J., Green, E. H., Kasibhatla, P., Eyring, V., and Lauer, A.: Mortality from Ship Emissions: A Global Assessment,  
397 *Environmental Science & Technology*, 41, 8512-8518, <http://dx.doi.org/10.1021/es071686z>, 2007b.
- 398 DJI S800-evo: <http://www.dji.com/product/spreading-wings-s800-evo>, 2014.
- 399 Eyring, V., Köhler, H. W., van Aardenne, J., and Lauer, A.: Emissions from international shipping: 1. The last 50 years, *Journal of*  
400 *Geophysical Research: Atmospheres*, 110, D17305, 10.1029/2004JD005619, 2005.
- 401 Fierz, M., Burtscher, H., Steigmeier, P., and Kasper, M.: Field measurement of particle size and number concentration with the Diffusion  
402 Size Classifier (DiSC), SAE Technical Paper, 2008.
- 403 Fuglestad, J., Berntsen, T., Eyring, V., Isaksen, I., Lee, D. S., and Sausen, R.: Shipping Emissions: From Cooling to Warming of Climate—  
404 and Reducing Impacts on Health, *Environmental Science & Technology*, 43, 9057-9062, 10.1021/es901944r, 2009.
- 405 Gonzalez, F., Castro, M. P. G., Narayan, P., Walker, R., and Zeller, L.: Development of an autonomous unmanned aerial system to collect  
406 time-stamped samples from the atmosphere and localize potential pathogen sources, *Journal of Field Robotics*, 28, 961-976,  
407 10.1002/rob.20417, 2011.
- 408 Hak, C. S., Hallquist, M., Ljungström, E., Svane, M., and Pettersson, J. B. C.: A new approach to in-situ determination of roadside particle  
409 emission factors of individual vehicles under conventional driving conditions, *Atmospheric Environment*, 43, 2481-2488,  
410 <http://dx.doi.org/10.1016/j.atmosenv.2009.01.041>, 2009.
- 411 Hallquist, Å. M., Fridell, E., Westerlund, J., and Hallquist, M.: Onboard Measurements of Nanoparticles from a SCR-Equipped Marine  
412 Diesel Engine, *Environmental Science & Technology*, 47, 773-780, <http://dx.doi.org/10.1021/es302712a>, 2013a.
- 413 Hallquist, Å. M., Fridell, E., Westerlund, J., and Hallquist, M.: Onboard Measurements of Nanoparticles from a SCR-Equipped Marine  
414 Diesel Engine, *Environmental Science & Technology*, 47, 773-780, 10.1021/es302712a, 2013b.
- 415 Hobbs, P. V., Garrett, T. J., Ferek, R. J., Strader, S. R., Hegg, D. A., Frick, G. M., Hoppel, W. A., Gasparovic, R. F., Russell, L. M., and  
416 Johnson, D. W.: Emissions from ships with respect to their effects on clouds, *Journal of the atmospheric sciences*, 57, 2570-2590, 2000.
- 417 Inc., P.: Picarro G2401 Analyzer. 2017.
- 418 Isakson, J., Persson, T. A., and Selin Lindgren, E.: Identification and assessment of ship emissions and their effects in the harbour of  
419 Göteborg, Sweden, *Atmospheric Environment*, 35, 3659-3666, [http://dx.doi.org/10.1016/S1352-2310\(00\)00528-8](http://dx.doi.org/10.1016/S1352-2310(00)00528-8), 2001.



420 Jayaratne, E. R., Ristovski, Z. D., Meyer, N., and Morawska, L.: Particle and gaseous emissions from compressed natural gas and ultralow  
421 sulphur diesel-fuelled buses at four steady engine loads, *Science of The Total Environment*, 407, 2845-2852,  
422 <http://dx.doi.org/10.1016/j.scitotenv.2009.01.001>, 2009.

423 Juwono, A. M., Johnson, G. R., Mazaheri, M., Morawska, L., Roux, F., and Kitchen, B.: Investigation of the airborne submicrometer particles  
424 emitted by dredging vessels using a plume capture method, *Atmospheric Environment*, 73, 112-123,  
425 <http://dx.doi.org/10.1016/j.atmosenv.2013.03.024>, 2013.

426 Kasper, A., Aufdenblatten, S., Forss, A., Mohr, M., and Burtscher, H.: Particulate Emissions from a Low-Speed Marine Diesel Engine,  
427 *Aerosol Science and Technology*, 41, 24-32, <http://dx.doi.org/10.1080/02786820601055392>, 2007.

428 Lack, D., Lerner, B., Granier, C., Baynard, T., Lovejoy, E., Massoli, P., Ravishankara, A. R., and Williams, E.: Light absorbing carbon  
429 emissions from commercial shipping, *Geophysical Research Letters*, 35, L13815, <http://dx.doi.org/10.1029/2008GL033906>, 2008.

430 Lack, D. A., Corbett, J. J., Onasch, T., Lerner, B., Massoli, P., Quinn, P. K., Bates, T. S., Covert, D. S., Coffman, D., Sierau, B., Herndon,  
431 S., Allan, J., Baynard, T., Lovejoy, E., Ravishankara, A. R., and Williams, E.: Particulate emissions from commercial shipping: Chemical,  
432 physical, and optical properties, *Journal of Geophysical Research: Atmospheres*, 114, D00F04, <http://dx.doi.org/10.1029/2008JD011300>,  
433 2009.

434 Lack, D. A., Cappa, C. D., Langridge, J., Bahreini, R., Buffaloe, G., Brock, C., Cerully, K., Coffman, D., Hayden, K., Holloway, J., Lerner,  
435 B., Massoli, P., Li, S.-M., McLaren, R., Middlebrook, A. M., Moore, R., Nenes, A., Nuaaman, I., Onasch, T. B., Peischl, J., Perring, A.,  
436 Quinn, P. K., Ryerson, T., Schwartz, J. P., Spackman, R., Wofsy, S. C., Worsnop, D., Xiang, B., and Williams, E.: Impact of Fuel Quality  
437 Regulation and Speed Reductions on Shipping Emissions: Implications for Climate and Air Quality, *Environmental Science & Technology*,  
438 45, 9052-9060, 10.1021/es2013424, 2011.

439 Malaver Rojas, J. A., Gonzalez, L. F., Motta, N., Villa, T. F., Etse, V. K., and Puig, E.: Design and flight testing of an integrated solar  
440 powered UAV and WSN for greenhouse gas monitoring emissions in agricultural farms, *International Conference on Intelligent Robots and*  
441 *Systems, Big Sky, Montana, USA, 2015 IEEE/RSJ*, 2015, 1-6,

442 Mazaheri, M., Johnson, G. R., and Morawska, L.: Particle and Gaseous Emissions from Commercial Aircraft at Each Stage of the Landing  
443 and Takeoff Cycle, *Environmental Science & Technology*, 43, 441-446, 10.1021/es8013985, 2009.

444 Mueller, L., Jakobi, G., Czech, H., Stengel, B., Orasche, J., Arteaga-Salas, J. M., Karg, E., Elsasser, M., Sippula, O., Streibel, T., Slowik, J.  
445 G., Prevot, A. S. H., Jokiniemi, J., Rabe, R., Hamdorf, H., Michalke, B., Schnelle-Kreis, J., and Zimmermann, R.: Characteristics and  
446 temporal evolution of particulate emissions from a ship diesel engine, *Applied Energy*, 155, 204-217,  
447 <http://dx.doi.org/10.1016/j.apenergy.2015.05.115>, 2015.

448 Murphy, S., Agrawal, H., Sorooshian, A., Padró, L. T., Gates, H., Hersey, S., Welch, W. A., Jung, H., Miller, J. W., Cocker Iii, D. R., Nenes,  
449 A., Jonsson, H. H., Flagan, R. C., and Seinfeld, J. H.: Comprehensive simultaneous shipboard and airborne characterization of exhaust from  
450 a modern container ship at sea, *Environ. Sci. Technol.*, 43, 4626-4640, <http://dx.doi.org/10.1021/es802413j>, 2009.

451 Petzold, A., Hasselbach, J., Lauer, P., Baumann, R., Franke, K., Gurk, C., Schlager, H., and Weingartner, E.: Experimental studies on particle  
452 emissions from cruising ship, their characteristic properties, transformation and atmospheric lifetime in the marine boundary layer, *Atmos.*  
453 *Chem. Phys.*, 8, 2387-2403, 10.1029/2004GL020312, 2008.

454 Petzold, A., Weingartner, E., Hasselbach, J., Lauer, P., Kurok, C., and Fleischer, F.: Physical properties, chemical composition, and cloud  
455 forming potential of particulate emissions from a marine diesel engine at various load conditions, *Environ. Sci. Technol.*, 44, 3800-3805,  
456 <http://dx.doi.org/10.1021/es903681z>, 2010.

457 Pirjola, L., Pajunoja, A., Walden, J., Jalkanen, J. P., Rönkkö, T., Kousa, A., and Koskentalo, T.: Mobile measurements of ship emissions in  
458 two harbour areas in Finland, *Atmospheric Measurement Techniques*, 7, 149-161, <http://dx.doi.org/10.5194/amt-7-149-2014>, 2014.

459 Reda, A. A., Schnelle-Kreis, J., Orasche, J., Abbaszade, G., Lintelmann, J., Arteaga-Salas, J. M., Stengel, B., Rabe, R., Harndorf, H., Sippula,  
460 O., Streibel, T., and Zimmermann, R.: Gas phase carbonyl compounds in ship emissions: Differences between diesel fuel and heavy fuel oil  
461 operation, *Atmospheric Environment*, 112, 370-380, <http://dx.doi.org/10.1016/j.atmosenv.2015.03.057>, 2015.

462 Ristovski, Z. D., Miljevic, B., Surawski, N. C., Morawska, L., Fong, K. M., Goh, F., and Yang, I. A.: Respiratory health effects of diesel  
463 particulate matter, *Respirology*, 17, 201-212, <http://dx.doi.org/10.1111/j.1440-1843.2011.02109.x>, 2012.

464 Schreier, S. F., Peters, E., Richter, A., Lampel, J., Wittrock, F., and Burrows, J. P.: Ship-based MAX-DOAS measurements of tropospheric  
465 NO<sub>2</sub> and SO<sub>2</sub> in the South China and Sulu Sea, *Atmospheric Environment*, 102, 331-343, <http://dx.doi.org/10.1016/j.atmosenv.2014.12.015>,  
466 2015.

467 Sinha, P., Hobbs, P. V., Yokelson, R. J., Christian, T. J., Kirchstetter, T. W., and Bruitjes, R.: Emissions of trace gases and particles from  
468 two ships in the southern Atlantic Ocean, *Atmospheric Environment*, 37, 2139-2148, [http://dx.doi.org/10.1016/S1352-2310\(03\)00080-3](http://dx.doi.org/10.1016/S1352-2310(03)00080-3),  
469 2003.

470 Streets, D. G., Carmichael, G. R., and Arndt, R. L.: Sulfur dioxide emissions and sulfur deposition from international shipping in Asian  
471 waters, *Atmospheric Environment*, 31, 1573-1582, [http://dx.doi.org/10.1016/S1352-2310\(96\)00204-X](http://dx.doi.org/10.1016/S1352-2310(96)00204-X), 1997.

472 UNCTAD: Review of Maritime Transport 2015, United Nations Conference on Trade and Development UNCTAD, 2015.

473 USEPA-OTAC: USEPA-OTAC, 2012. <http://www.epa.gov/otaq/oceanvessels.htm#regs>, Ocean Vessels and Large Ships. US  
474 Environmental Protection Agency, Office-of-Transportation-and-Air-Quality. , 2012.

475 Viana, M., Hammingh, P., Colette, A., Querol, X., Degraeuwe, B., Vlioger, I. d., and Van Aardenne, J.: Impact of maritime transport  
476 emissions on coastal air quality in Europe, *Atmospheric Environment*, 90, 96-105, <http://dx.doi.org/10.1016/j.atmosenv.2014.03.046>, 2014.

477 Westerlund, J., Hallquist, M., and Hallquist, Å. M.: Characterization of fleet emissions from ships through multi-individual determination  
478 of size-resolved particle emissions in a coastal area, *Atmospheric Environment*, 112, 159-166,  
479 <http://dx.doi.org/10.1016/j.atmosenv.2015.04.018>, 2015.

480 WHO: Review of evidence on health aspects of air pollution 2013.

481 Williams, E. J., Lerner, B. M., Murphy, P. C., Herndon, S. C., and Zahniser, M. S.: Emissions of NO<sub>x</sub>, SO<sub>2</sub>, CO, and HCHO from commercial  
482 marine shipping during Texas Air Quality Study (TexAQ5) 2006, *Journal of Geophysical Research: Atmospheres*, 114, D21306,  
483 10.1029/2009JD012094, 2009.

484 Winnes, H., Moldanová, J., Anderson, M., and Fridell, E.: On-board measurements of particle emissions from marine engines using fuels  
485 with different sulphur content, *Proc. Inst. Mech. Eng. Part M J. Eng. Marit. Environ.*, 230, 45-54, 10.1177/1475090214530877, 2016.



# Copernicus Publications

The Innovative Open Access Publisher